MAGNETICALLY RESPONSIVE DROPLET INTERFACE BILAYER NETWORKS

by

KHUSHBOO DEVANG BRAHMBHATT

(Under the Direction of Eric Freeman)

ABSTRACT

This work explores incorporating ferrofluids into droplet interface bilayer (DIB) networks, using magnetic nanoparticles for the arrangement and creation of complex membrane networks and their remote mechanical manipulation. First, a suitable biocompatible ferrofluid is developed. DIBs between droplets containing the ferrofluid are constructed, with both symmetric and asymmetric distributions of the ferrofluid in the droplets and their stability and quality are assessed. The response of the individual droplets is dependent on their ferrofluid composition, leading to complex self-assembly behaviors of cellular networks. Strategies for controlling the formation of these networks are examined and discussed. Developing a more rapid solution for creating complex DIB networks may open the door for applying this technique to study transmembrane proteins, creating a biologically adaptive material, and perhaps advancing the field towards the tissue scale in the future.

INDEX WORDS: Ferrofluid, Droplet Interface Bilayer, Lipids, SPION

MAGNETICALLY RESPONSIVE DROPLET INTERFACE BILAYER NETWORKS

by

KHUSHBOO DEVANG BRAHMBHATT

B.S., The University of Georgia, 2012

A Thesis Submitted to the Graduate Faculty of The University of Georgia in Partial Fulfillment of the Requirements for the Degree

MASTER OF SCIENCE

ATHENS, GEORGIA

2016

MAGNETICALLY RESPONSIVE DROPLET INTERFACE BILAYER NETWORKS

by

KHUSHBOO DEVANG BRAHMBHATT

Major Professor:	Eric Freeman
Committee:	Leidong Mao Mark Haidekker

Electronic Version Approved:

Suzanne Barbour
Dean of the Graduate School
The University of Georgia
May 2016

DEDICATION

I would like to dedicate this work to:

My mom and dad, Chetna and Devang, thank you for your continuing support in my life decisions and always encouraging me to achieve my dreams.

My sister and brother, Reshma and Frankie, thank you for helping me keep my sanity! We are siblings by blood, but friends by choice.

Mikhail, thank you for being such a positive force in my life and helping me in any way you could whether it be proofreading papers to alphabetizing my students' quizzes. I love you!

And Kevin and Betsy, you have NO idea how much you've helped me these past years. From having Sadie over multiple times a week to helping my craft my teaching philosophy and everything in between, I thank you!

ACKNOWLEDGEMENTS

I would like to acknowledge:

My advisor, mentor, and principal investigator, Dr. Eric Freeman. I cannot even fathom having a better advisor. The guidance and advice you've given me over the years is invaluable. Thank you for the opportunity to work in your lab.

Drs. Leidong Mao and Mark Haidekker for your service on my committee.

TABLE OF CONTENTS

Page

LIST OF TABLES

Page

LIST OF FIGURES

Page

CHAPTER 1

OVERVIEW

1.1 Purpose of Study

This study explores incorporating ferrofluid with droplet interface bilayer (DIB) membranes. Ferrofluids contain dispersed superparamagnetic nanoparticles (SPION) coated in with a stabilizing surfactant in a solution, providing a magnetically-responsive fluid. These nanoparticles provide a platform for remote mechanical manipulation of ferrofluid droplets by applying an external magnetic field and would allow for better control over the characteristics of networks of stimuli-responsive cellular membranes created through the DIB technique. The magnetic property of ferrofluid would also allow for rapid assembly of large networks which has posed to be a very tedious and time consuming task. In order to guarantee that the ferrofluid would not interfere *in vivo*, should this technique be used for biological purposes, a suitable biocompatible ferrofluid is synthesized containing a biocompatible surfactant. Once it is confirmed that the ferrofluid droplets do not negatively interfere with the formation of the artificial cellular membranes through the electrical measurements of membrane properties and interfacial tension measurements, the magnetically-responsive nature of the ferrofluid droplets are used to form large networks of DIB membranes through a simple magnetic field. These networks are easy to assemble and may be remotely manipulated, providing a significant

step towards the rapid and simple assembly of DIB networks advancing towards the tissue scale.

CHAPTER 2

INTRODUCTION

2.1 Phospholipids and Artificial Bilayers

Phospholipids are a subclass of lipids that are the building blocks to forming cellular membranes [2]. Phospholipids are amphiphilic in nature meaning they are made up two hydrophobic fatty acid tails and a hydrophilic polar head group. When these lipids are allowed time to self-assemble at the interface of two phases (in the author's case, water and oil) a lipid monolayer is formed (Figure 1) and when two of these monolayers are brought into contact, the hydrophobic tails appear to zip together to form what is known as a lipid bilayer. These bilayers are typically ~5nm in thickness and are impermeable to most water soluble molecules and ions [3].

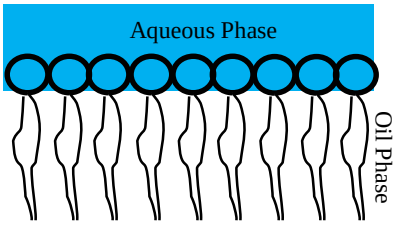

Figure 1: This schematic represents the formation of a monolayer. Hydrophilic heads of the lipid self-assemble to the aqueous phase of the interface and the hydrophobic tails remain in the oil phase.

Over the years there have a few different methods in creating artificial bilayer models to mimic biological cell membranes. Artificial bilayers are easier to form and to work with compared to the process it takes to extract a membrane from a real biological cell. The ability to create artificial bilayers has allowed for in depth studies on the fundamental properties of lipid bilayers such as thickness [4], capacitance and resistance [5-8], surface tension effects [8], as well as mechanical properties [9, 10]. The earliest

artificial bilayer model developed is referred to as black lipid membranes (BLM) and was first reported in 1963 [11]. To form a BLM a sheet of plastic with a small aperture in the center separates the two sides of a chamber that is filled with a solvent (usually a mixture of decane and squalene). The area around the aperture is first treated with a solution of lipids dissolved in a hydrophobic solvent by applying this solution across the aperture with a brush, syringe, or glass applicator [12]. The bilayer is formed across the aperture, separating the two chambers (Figure 2). The electrical properties of the bilayer can be measured by placing an electrode into each side of the separated chamber. The term "black" lipid membrane refers to the fact that they are dark in reflected light because the thickness of the membrane is only a few nanometers, so light reflecting off the back face destructively interferes with light reflecting off the front face which was a visual clue to the confirm that a membrane of molecular thickness was created. The main problems associated with the BLM are residual solvent and limited lifetime. The solvent in the chambers in this method are trapped in a V-shaped gap between the two sheets of plastic which will interfere with normal protein function should this method be used to study membrane proteins. To overcome this limitation, Montal and Mueller developed a modified technique that eliminates the use of

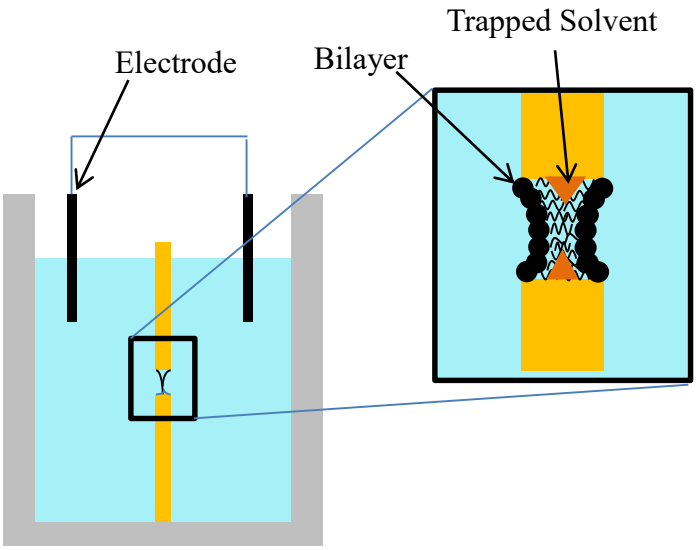

Figure 2: Set up to create a BLM bilayer. Bilayer is formed across the aperture in a separated chamber.

a heavy non-volatile solvent [13]. This time the aperture starts out above the water surface and completely separates the two fluid chambers. On the surface of each chamber, a monolayer is formed by applying lipids in a volatile solvent, such as chloroform, and waiting for the solvent to evaporate. The sheet with the aperture is then lowered and the two monolayers from the separate chambers are folded down against each other, forming a bilayer across the aperture. This method of creating a BLM eliminated the problem of trapped solvent; however, the problem of stability was still a pressing issue. BLM bilayers only last for a few hours and any holes in the membrane can cause failure. This issue can be resolved by forming a bilayer using the supported lipid bilayer (SLB) method. SLBs are a planar bilayer in which only one monolayer is exposed to the solvent and the other is supported on wetted substrate. These bilayers are significantly more stable than BLM bilayers and failure does not occur for several weeks. Further increases in stability are shown by using a tethered bilayer lipid membrane (t-BLM). The stability is increased by chemically anchoring the lipids to the substrate.

2.2 Droplet Interface Bilayer

The spontaneous bilayer that forms at the interface of two or more lipid monolayer-coated aqueous droplets is called a droplet interface bilayer (DIB). These bilayers have several advantages over previous planar bilayers often created by the Montal-Muller method [13]. DIBs are significantly stronger and more stable than planar bilayers. DIBs can be separated and reform with little effort. There are a couple

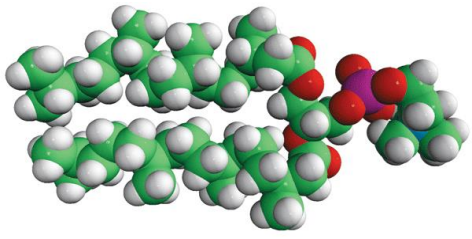

Figure 3: Courtesy of Avanti Polar Lipids. Molecular representation of the lipid used in this work, 1,2-diphytanoyl-sn-glycero-3-phosphocholine (DPhPC).

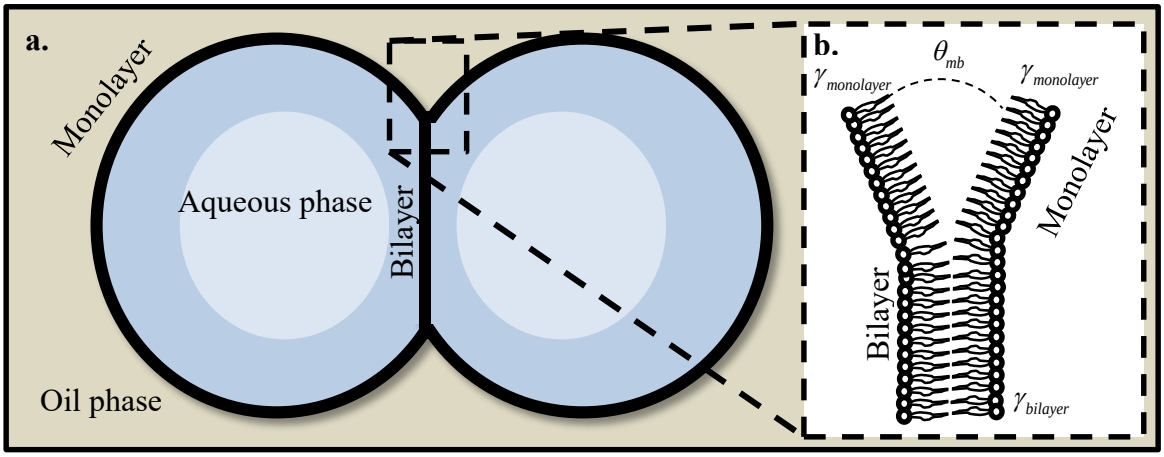

Figure 4: Modified from [1]. The droplet interface bilayer (DIB) approach. Lipids are used as organic surfactants, coating aqueous droplets in oil. Bringing the lipid-coated droplets into contact creates stable interfacial membranes that mimic cellular membranes.

different ways to form the lipid monolayer that encloses the aqueous droplets of DIBs. The "lipid-in-oil" or "lipid out" technique uses lipids dissolved in the continuous oil phase [14-16]. The "lipid-in-water" or "lipid-in" technique dissolves the lipids in the aqueous phase [17]. They migrate to the oil-water interface at the droplet surface and self-assemble into an ordered lipid monolayer, acting as a natural surfactant and reducing the surface tension of the droplets. When these droplets are brought into contact, the hydrophobic tails of the lipids zip together and expel the oil between the droplets to create a stable interfacial membrane (Figure 4). There have been a few studies to claim to have discovered DIBs. In 2006 Takeuchi et al. reported an artificial lipid bilayer at the interface of two lipid monolayer coated aqueous droplets[16]. In 2007 Bayley *et al*. reported the term DIB and functional bionetworks using DIBs [14]. Single nano pore insertions, bio battery, light sensing, and pore blocker screening were reported. In another journal article, Bayley *et al*. reported electrical modeling for DIB networks with nano pores using SPICE simulations, validating experimentally [15]. In 2008 Bayley *et al*.

reported a modified approach for forming DIBs that allows asymmetric bilayers to form in DIB [17]. Also, that lipids can be contained as vesicles inside aqueous droplets rather than in surrounding oil. Bayley *et al*. summarized DIB relevant research work till 2008 in a review paper [18]. Leo et al. reported tailored current-voltage relationships in DIB containing voltage gated alamethicin nanopores [19]. Another group led by Lavan *et al* reported DIB as a synthetic protocell for energy conversion and mimic a biological battery [20]. An ion gradient was maintained across the DIB by varying saline concentration in individual DIB forming droplets. Nanopores in DIB acted as nano conductors for ions across DIB. In 2010 Leo *et al*. reported non-invasive measurement techniques using a physical encapsulation technique to withstand high accelerations, inversion, and shaking for DIBs and a water swollen hydrogel based mimic of DIB [21-23]. While most of the DIB researchers used only DPhPC lipid, Ces *et al*. demonstrated the use of DOPC lipid as well [24]. Complex three dimensional DIB networks are shown to be stable. Other relevant reports include Tsofina *et al*. who reported the formation of lipid bilayer in lipid-heptane bath by contacting two lipid monolayer coated aqueous interfaces against each other [25].

DIBs are an ideal model membrane to study transmembrane proteins [26]. Membrane proteins may be deposited in the aqueous phase allowing for their incorporation into the DIB. By incorporating membrane proteins, ion channels, pores, and pumps, networks of bilayers may be engineered to simulate biological processes. Larger networks expanding towards the tissue scale will allow for the development of complex cellular networks through the inclusion of stimuli-responsive biological pores and channels inserted at the interfacial membrane. DIB networks have been designed to

act as simple functional electronic circuits to create networks capable of sensing light and acting as bio-batteries [13-15].

2.3 Current Limitations

Most of the studies outlined in the previous section utilized DIBs for in depth studies on lipid bilayers. To fully explore the extent of applications of DIB networks, automated methods for creating extensive networks needs to be created. The ability to create large networks will allow for the creation of protocells that can be used to mimic many biological systems in our body. Currently the method for creating an extensive network is a tedious and time consuming process and manipulation of the network after creation is similarly challenging. In order to create a network each aqueous droplet is micro pipetted into the continuous phase (usually oil). After a few minutes has passed to allow for monolayer formation, each droplet then is manually brought into contact using a micromanipulator. As the size of the network increases, the amount of time dedicated to the creation of the network increases as well since each droplet must be brought into contact individually. Previous research has been done to try to address some of the limitations of the traditional DIB method for network creation. The use of a magnetic beads in the aqueous phase has been studied to provide the ability to remotely manipulate the droplets once in the oil bath [27]. The magnetic beads allows for the creation of 2D and 3D networks by using the levitation technique. A magnetic rod is used to remotely maneuver droplets into contact to form the interconnected membranes. The creation of the droplets is still manually done by pipetting the droplets, and then the droplets loaded with the magnetic beads, which in itself can be a tedious process. Even though this study shows that utilizing magnetic properties is a possible solution for remote manipulation,

the ability to create droplets in large quantities is still an issue that needs to be addressed. 3D printing [28] and microfluidics [29] has been studied as possible solutions to creating a large volume of droplets; however, these techniques do not address the previous problem of remote manipulation. The goal of this thesis work is to provide a solution to create a large extensive network in a short amount of time to propel further research on DIBs to its full potential.

2.4 Ferrofluid

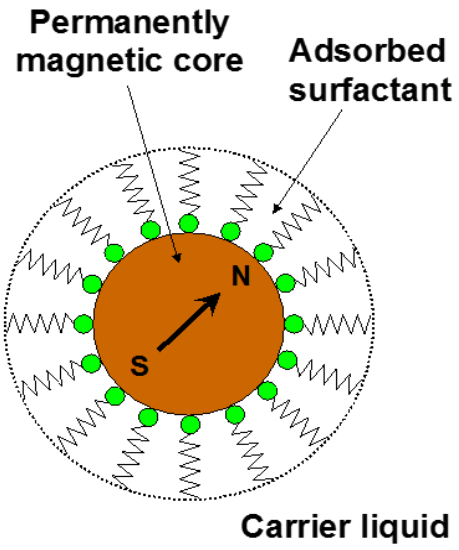

Figure 5: Magnetic nanoparticle cores are generated and coated with a surfactant to maintain dispersion in the fluid.

In order to remedy the issue of creating large networks, this thesis work focuses on incorporating ferrofluid into the aqueous phase to make network assembly as simple as exposing the droplets to a permanent magnet in the desired location/ Ferrofluid also provides a macroscopically continuous magnetic fluid phase, which makes it an ideal candidate for microfluidic applications to streamline the formation of the droplets.

Ferrofluids have a wide range of applicable potential in the field of biomedicine, including cellular manipulation [30] and sorting [31, 32], hyperthermia [33, 34] and targeted drug delivery [35, 36]. Ferrofluids are colloidal suspensions comprised of nanosized magnetic particles that are stabilized with a surfactant. It is mainly composed of synthetic γ-Fe_2O_3, known as maghemite, or Fe_3O_4, known as magnetite (Figure 5). These nanoparticles are suspended in a carrier liquid, typically deionized water, and can be coated with different polymers or other surfactants. The surfactant layer helps overcome the Van der Waal's forces by preventing the particles from agglomerating, either via steric or electrostatic repulsions. The nanoparticles in ferrofluid are also known as superparamagnetic iron oxide nanoparticles (SPION). Superparamagnetism is a form of magnetism, which appears in small ferrous nanoparticles. In sufficiently small nanoparticles, magnetization can randomly flip direction under the influence of

temperature [37]. As a result, the fluid quickly loses its magnetization when the external magnetic field is removed from the particles. There are many factors to consider when creating SPION, such as the pH, particle size, and surface properties. Each of these alters the physiochemical properties of the ferrofluid. In biomedical applications particle agglomeration *in vivo* may even lead to dangerous scenarios, such as artery blockages and tissue damage.

2.5 Goal of Thesis

The purpose of this thesis is to provide a protocol for forming extensive DIB networks in a far less time consuming and tedious method. In order to accomplish this goal, this work will explore the effects of incorporating ferrofluid into the aqueous phase of a DIB. This thesis is organized by chapters that will characterize the ferrous DIB. Chapter 3 highlights the biocompatibility of the ferrofluid used throughout the thesis work and will also discuss the possibility of DIB networks as an adaptive biologically inspired material. Chapter 4 focuses on characterizing a ferrous DIB membrane using specific capacitance measurements. Chapter 5 includes experiments done on characterizing ferrous DIB networks and studies the capabilities of ferrous networks. Chapter 6 will discuss options for pre and post assembly manipulation. The possibility of asymmetrical membranes (membranes formed between one or more ferrous droplets and one or more aqueous droplets) to allow for protein or channel incorporation is also evaluated. In chapter 7 the process of characterizing the surface tension or interfacial tension (IFT) of the droplets is outlined. And finally Chapter 8 will discuss the thesis work as a whole and conclude with recommendations for further research.

CHAPTER 3

BIOCOMPATIBLE FERROFLUID

3.1 Biocompatible Coating in DIB Formation

There are a number of different surfactants that can be used to coat the SPION in ferrofluid. The two most frequently used biocompatible surfactants in these experiments include polyethylene glycol (PEG) and polymethyl methacrylate (PMMA). Our lab was gifted various ferrofluids coated with PEG and PMMA from the Laboratory of Magnetism for Biomedical Research at UGA. With these ferrofluid we ran numerous tests to assess their suitability for the magnetic application of DIB networks. The first test was to see if ferrofluid and lipids together in the aqueous phase could form membranes. It was quickly discovered that using the lipid-in-water approach with ferrofluid would pose many issues. The lipids dissolved in the aqueous phase would not self-assemble themselves correctly when ferrofluid was introduced. It is likely that the lipids were trying to insert themselves onto the surfactant coated SPION, or the distance between the nanoparticles was insufficient for liposome migration to the oil-water interface. Then a lipid-in-oil approach was taken instead, this approach showed very healthy and robust membranes. It was also observed that uncoated ferrofluid with low pH values could even create membranes. This is an interesting occurrence noting that the acidic environment posed by the ferrofluid did not have an adverse effect on membrane formation; however,

for this and the following studies, a biocompatible ferrofluid must be used to allow this technique to be used in medical applications.

3.2 Ferrofluid Characterization

The aim of this section is to characterize the ferrofluid that was used in this thesis work. Size distribution and morphology of the maghemite nanoparticles were investigated via Transmission Electron Microscopy (TEM; FEI Tecnai 20, Hillsboro, OR) (Figure 6a). Magnetic properties of the ferrofluid were measured at room temperature using a Vibrating Sample Magnetometer (VSM, Model EZ7; MicroSense, LLC, Lowell, MA) with a 2.15 T electromagnet. The typical size of the magnetic particles is ~10nm including the surfactant material (which is around 2nm thick) (Figure 6a). This makes the particles sufficiently small to be considered magnetic mono-domains, which is an important characteristic, because the particles have to have non-zero magnetic moments for the ferrofluid to show its magnetic properties [38]. The magnetic moment of ferrofluid was measured over a range of applied fields from -21.5 to +21.5 kOe. When an external magnetic field is applied to ferromagnetic substances, the atomic dipoles align themselves with it. Even when the field is removed, part of the alignment can be retained and the substance has become magnetized. This phenomenon is known as magnetic hysteresis. Since ferrofluid is made up of SPION which have superparamagnetic properties, there is no hysteresis in ferrofluid which is clear from the lack of a hysteresis loop in the graph (Figure 6c). This is an important characteristic of ferrofluid that make it attractive to use in the biomedical field. The volume fraction of a ferrofluid, denoted by Φ, is the volume percentage of magnetic solid material with respect to the total volume including the carrier fluid and the surfactant [39]. A biocompatible PEG stabilized

ferrofluid of volume fraction ~1% and PMMA stabilized volume fraction 0.5% were used for the experiments.

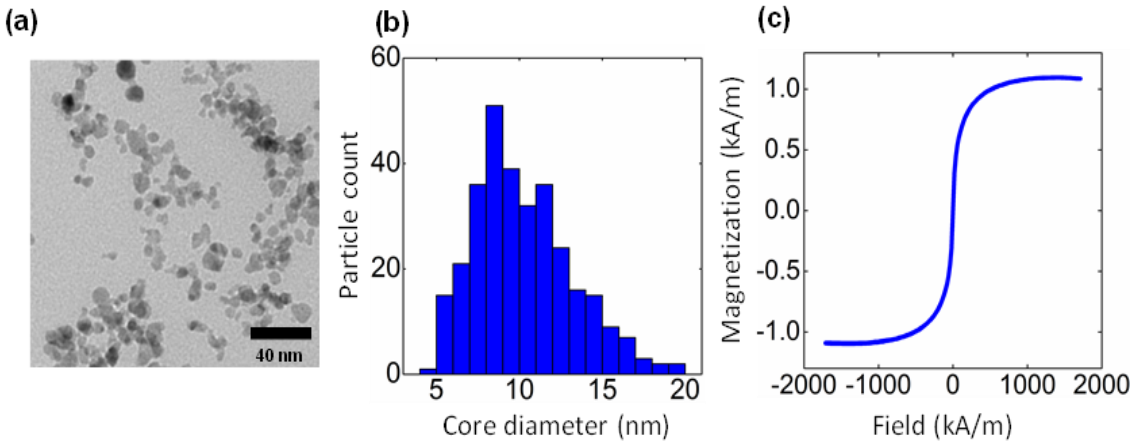

Figure 6: Characterization of the ferrofluid particles, including TEM imaging (a), particle diameter analysis (b), and magnetization (c).

CHAPTER 4

MEMBRANE CHARACTERIZATION

4.1 Overview

After visual confirmation from the previous chapter, it was clear that a membrane was forming between two ferrous droplets. This chapter looks to confirm quantitatively that the ferrofluid was not interfering with the membrane formation on fundamental level specific capacitance measurements need to be taken. These measurements will then be compared to the capacitance measurements of an aqueous DIB. DIB allows for optically tracking the interfacial area between droplets and varying membrane area, in addition to permitting electrical measurements of membrane capacitance. Each interfacial membrane may be modeled as a four-node electrical circuit stencil (Figure 7) The lipid membrane operates as a natural capacitor in parallel with a low-conductivity resistor [14]. The membrane also possesses a set range of specific capacitances (capacitance per area) that may be linked to the thickness of the membrane. Measuring the specific capacitance of the membrane allows for a quick assessment of the membrane properties.

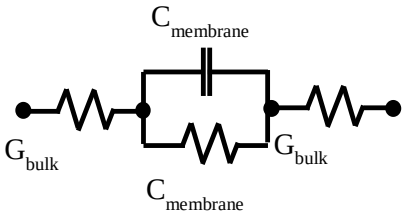

Figure 7: Four node stencil for a lipid bilayer membrane. C is the membrane capacitance; G represents the conductance of the aqueous solution and the membrane.

4.2 Materials and Methods

The tip of a pulled pipette (World Precision Instruments, P-1000, Sutter) is filled with ~0.5% PEG coated ferrofluid was placed in a petri dish (Ibidi) with a 50:50 mixture of hexadecane and silicone oil AR20 (Sigma Aldrich) with dissolved DPhPC phospholipids (Avanti). The ferro droplets were injected (Femtojet 4i, Eppendorf) onto agarose-coated Ag/AgCl electrodes submerged in the 50:50 oil mixture containing lipids. The electrodes were connected to a patch-clamp system (Multiclamp 700B, Digidata 1550, and Molecular Devices) and signal generator (Hewlett Packard 33120A). All measurements were taken inside of a Faraday cage to reduce external noise. For an image of the experimental set up please refer to Appendix A2 and A3. In order to calculate the specific capacitance, the experiment requires simultaneous measurement of both the membrane capacitance and the area of the bilayer (contact area between droplets). Membrane capacitance can be measured by the current induced by a triangular waveform voltage, while area is computed from a measurement of bilayer diameter from a picture taken at the same time as the electrical measurements are recorded. The two droplets were brought into contact using a manual micromanipulator and a 10 mV 10 Hz triangle wave signal was passed across the membrane (Figure 8b). The necessary current for maintaining the clamped membrane potential was recorded in voltage-clamp mode. As the electrical measurements were being recorded, an image of the droplets was taken. The droplet area was varied by pulling the droplets apart, reducing the equilibrium membrane area, and the capacitance measurements were repeated.

4.2.1 Specific Capacitance Measurements

To calculate the specific capacitance, first the diameters of the DIBs were visually assessed on the images by using scale bars in the Leica LASX software (Figure 8a). The diameter was measured at least three times per trial and averaged, and this diameter was used to estimate the area of the interfacial membrane. Once the areas were calculated, nominal capacitance was calculated using the current recorded and the capacitance may be estimated through the standard equation for capacitive current (Equation 1) and linked to the specific capacitance through the estimated membrane area (Equation 2). A 10mV 10 Hz triangle wave voltage was supplied to produce a constant dV/dt, allowing for measurements of the membrane capacitance.

$$i_{capacitive} = \frac{dV_{membrane}}{dt} C_{membrane} \qquad \text{Equation 1}$$

$$C_{spec} = \frac{C_{membrane}}{Area} \qquad \text{Equation 2}$$

4.3 Results and Conclusions

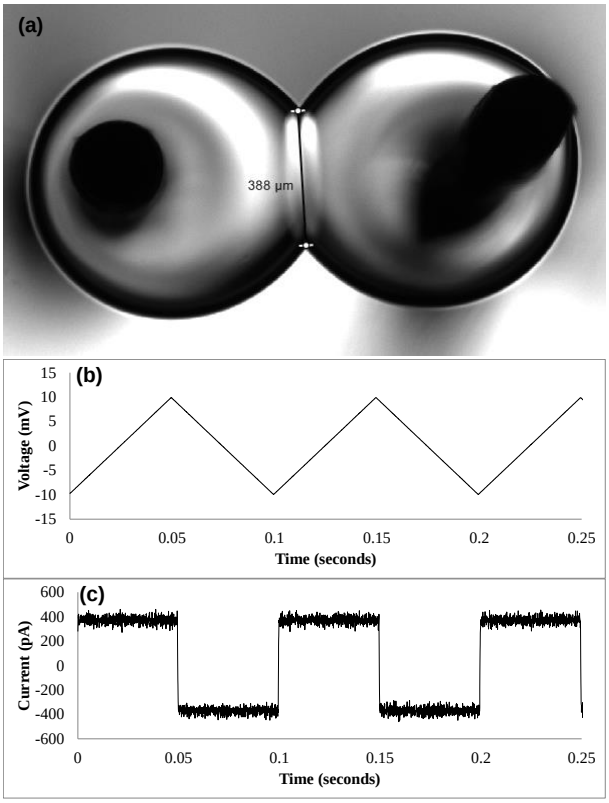

Figure 8: a) The diameter of the interfacial membrane is used to assume the total membrane area. This is combined with (b-c) capacitance measurements of the membrane, allowing for calculations of the specific capacitance.

Each scenario was tested in three separate trials with each trial containing four measurements. After membrane formation, the droplets were pulled apart decreasing the area of the membrane in slowly. This process was repeated four times for each trial. For the ferrous membrane, the membrane surface averaged at 258 µm at its largest and 116 µm at the smallest. For the aqueous membranes, the average surface at its largest was 432 µm and 393 µm at its smallest. From this the area, assuming a circular contact area, was calculated. The measured average specific capacitance of the ferrous DIB was $0.82 \pm 0.078 \mu F/cm^2$ and $0.77 \pm 0.078\ \mu F/cm^2$ for the aqueous droplets. These values are in close agreement with previously reported values of $0.65 \pm 0.2 \mu F/cm^2$ and $0.64 \pm 0.003 \mu F/cm^2$ for a DIB formed using hexadecane[8]. Since the oil we used was a 50:50 mixture of hexadecane and silicone oil, the capacitance results were slightly higher. However, given that lipid bilayers are known to exhibit specific capacitances between 0.5 and 1.0 µF/cm2 , this data provides evidence that the interface formed between the ferrofluid droplets is similar to non-ferrofluid

interfaces within a standard deviation of capacitance. The readings for all ferrofluid droplet cases showed a strong square-wave current response to the triangle wave voltage. The membrane area was stable, reaching equilibrium quickly, and the time to formation was typically less than 30 seconds.

CHAPTER 5

NETWORK CHARACTERIZATION

5.1 Overview

This chapter will characterize the stability, flexibility and capacitive current of ferrous networks. The magnetic property of ferrofluid is what made it an attractive solution to DIB network creation. Not only does it make it easier to assemble the network, but it provides a way to manipulate the network post assembly which previously could only be done by the use of manual micromanipulators. First the assembly of a large network configuration is assessed. The network is visually examined for leakage between membranes and the assembly process is tested for efficiency. Once a stable network is shown to form, another ferrous network is created to be stretched while electrical measurements are taken. The purpose of this is to help quantify the overall capacitive current of the network while it is being manipulated.

5.2 Network Stability

With the initial membrane characterization complete, the next step is utilizing the ferrofluid droplet response towards magnets for the construction of large DIB networks. The tip of a pulled pipette (World Precision Instruments, P-1000, Sutter) is filled with ~0.5% PEG coated ferrofluid was placed in a petri dish (Ibidi) with a 50:50 mixture of hexadecane

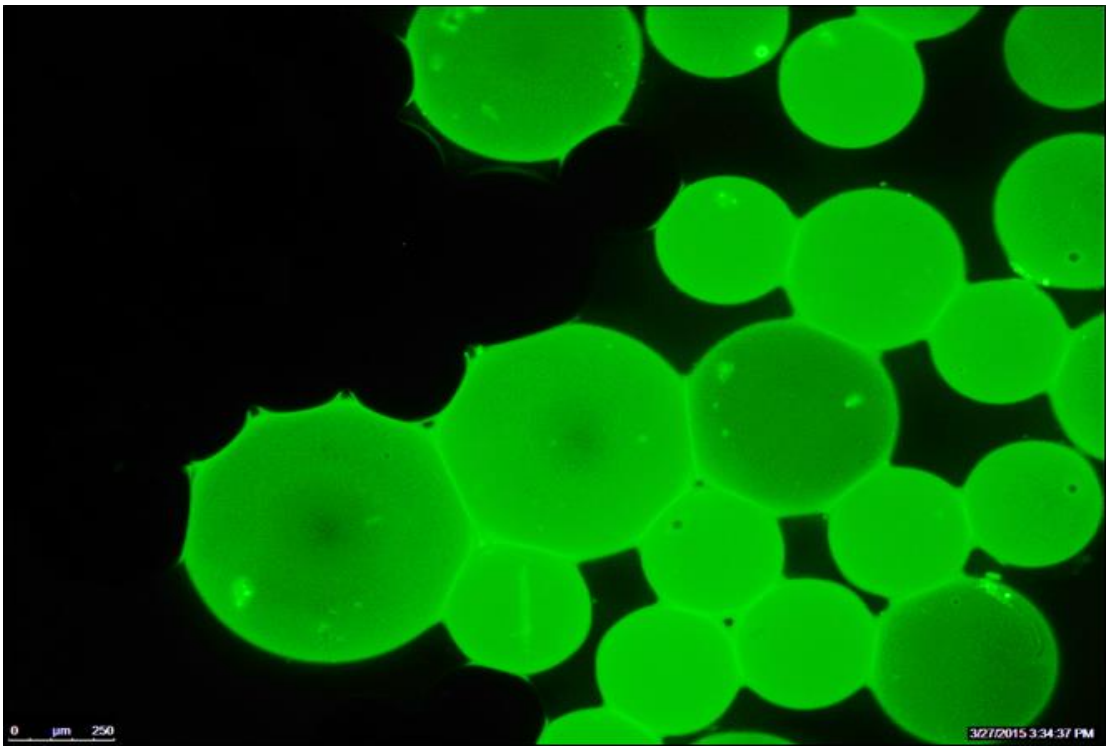

Figure 9: Rapidly assembled DIB network visualized with fluorescent microscopy, demonstrating stable membranes with no detected diffusion of dye.

and silicone oil AR20 (Sigma Aldrich) with dissolved DPhPC phospholipids (Avanti). The ferrous droplets of different sizes were injected (Femtojet 4i, Eppendorf) into the 50:50 oil mixture containing lipids. Another pipette was then filled with the same ferrofluid however, this time with fluorescein dye (1 mM, Sigma) was also deposited into the same petri dish. Numerous droplets of different sizes were arbitrarily deposited around the petri dish. A magnet was placed underneath the petri dish after the droplet deposition, pulling the ferrofluid droplets to the center directly above the magnet, allowing for the initial formation of interfacial DIB membranes at the contact areas between the ferrofluid droplets. The magnet was then removed from the dish after initial contact was established and the network continued to pull together, closing gaps and creating a compact DIB network. Clusters have been observed to be the lowest energy configuration for DIBs [40], so the network will continue to pull together until a locally

stable equilibrium is reached. By adding fluorescein dye in roughly half of the droplets, leakage between the membranes can be easily, visually assessed. From the fluorescence image obtained from an inverted brightfield microscope (Leica DMI3000B) in Figure 9 it is clear that there was no leakage of the dye between the membranes. The network assembly also was very rapid and took less than two minutes to reach equilibrium.

5.3 Network Stretching

Once it is proven that healthy, robust membranes can form a large network, the network itself needs to be assessed for flexibility and how the network reconfigures. The tip of a pulled pipette (World Precision Instruments, P-1000, Sutter) is filled with ~0.5% ferrofluid was placed in a petri dish (Ibidi) with a 50:50 mixture of hexadecane and silicone oil AR20 (Sigma Aldrich) with dissolved DPhPC phospholipids (Avanti). The ferro droplets were injected (Femtojet 4i, Eppendorf) in to the oil bath. A magnet was placed in the dish

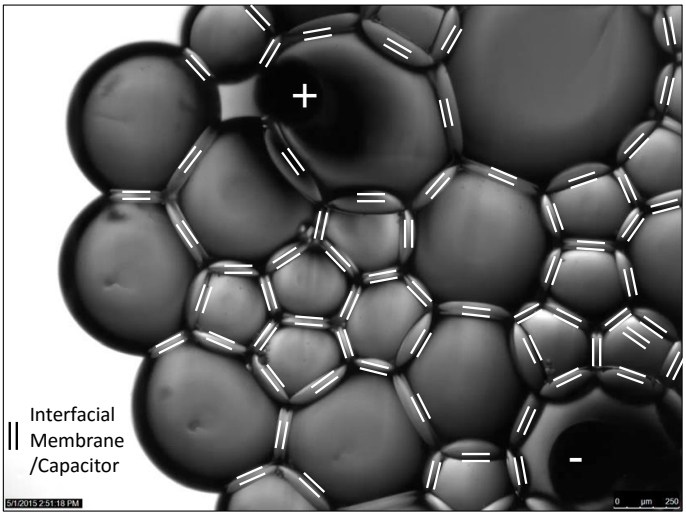

Figure 10: Image of a ferrofluid DIB network, punctured by agarose-coated Ag/AgCl electrodes. The droplets form a complex network of interfacial membranes which may be approximated as capacitors.

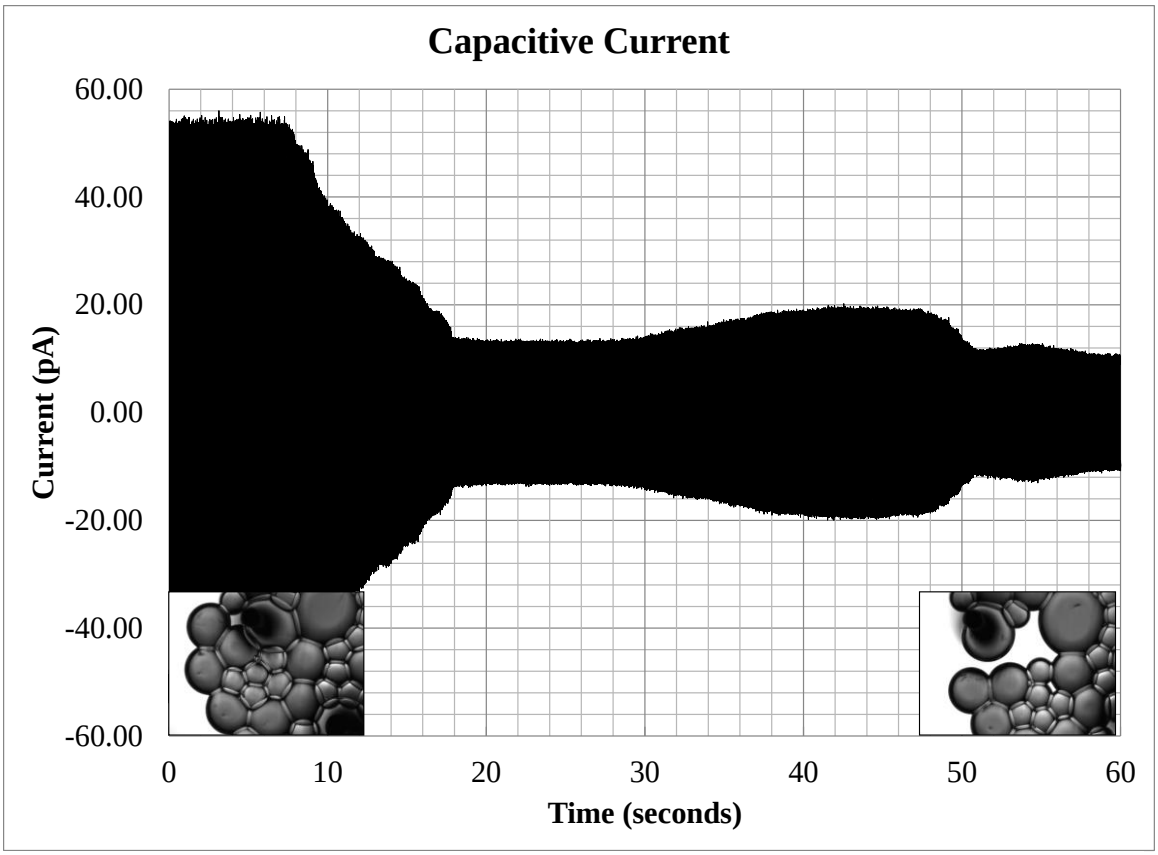

Figure 11: Mechanically stretching the network apart through the hydrophilic electrodes rearranges the network from a compact cluster to a chain, effectively reducing the overall capacitance. A stable square wave capacitance was recorded throughout in response to a 20 mV 10 Hz triangle wave voltage.

to center all the droplets above it. Once the droplets were in close proximity membrane formation occurred. The network was then punctured with Ag/AgCl electrodes attached to micromanipulators (Siskiyou) (Figure 10). The electrodes were connected to a patch-clamp system (Multiclamp 700B, Digidata 1550, and Molecular Devices) and signal generator (Hewlett Packard 33120A). All measurements were taken inside of a Faraday cage to reduce noise. Once the network reached an equilibrium configuration, electrical measurements were taken while the network was stretched by pulling apart the network using the micromanipulators. Each interfacial membrane may be modeled as a four-node electrical circuit stencil (Figure 7). This stencil may be combined to overlay complex networks of DIB membranes (Figure 10), providing an equivalent electrical circuit

description of the DIB network [41]. At low frequencies (< 100 Hz), the membrane may be approximated as a simpler capacitor. This is due to the conductivity ratio of the bulk solution and the membrane ($\approx 10^3$ to 10^{12} Ω [41]). The membrane structure may be viewed as a network of capacitors in parallel and in series, providing an equivalent capacitance that describes the current configuration of the network. The electrodes attached to the droplets are then pulled apart, separating multiple membranes and rearranging the microfluidic network. During this process the capacitive current drops as the individual membranes are separated as shown in Figure 11. The network was stretched for 18 seconds and then left to reach equilibrium and then after about 12 seconds the network was brought closer into contact to reconfigure and stretched again. From Figure 11 we can clearly see that the configuration of the network corresponds directly to the overall capacitive current. The ferrous network formed by the droplets is shifting from a compact cluster to a longer chain, which reduces the equivalent capacitance of the network. If the droplets are left undisturbed in the chain configuration, a gradual reformation of the membranes is observed as the droplets draw together, seeking the lowest energy configuration by maximizing the number of interfacial bilayer areas while remaining constrained by the electrodes.

5.4 Conclusion and Discussion

The stability, flexibility and capacitive current of ferrous networks were assessed in this chapter. By creating a network with fluorescein laden ferrous droplets and unmodified ferrous droplets a visual assessment for leakage was possible. The network formed with ease and required little time to reach equilibrium. Another network formed with the same protocol to measure the capacitive current of a network that is being manipulated. This

network showed incredible flexibility in reconfiguring once manipulated and stretched. The overall capacitive current decreases when the network is stretched and increases when the network reconfigures. Ferrous networks are shown to form stable, robust, and leak-proof membranes that are capable of being manually manipulated.

CHAPTER 6

REMOTE MANIPULATION

6.1 Overview

This chapter will look to tailor the volume fraction of the ferrofluid for remote manipulation and will also explore options in asymmetrical membranes. When a network is formed with aqueous droplets, it is difficult to move the network or change the configuration of the network. The possibility of remote manipulation would allow for a researcher to tailor a particular network either pre or post assembly. Ferrofluid provides a platform to accomplish this task, the purpose of providing a solution to network creation is to further the field of DIB research; however, the effects of SPION on membrane proteins, channels, and pores has not been assessed. By testing asymmetrical networks (networks consisting of both ferrous and aqueous droplets), the issue of SPION interference is eradicated. The use of a ferrous droplet as a "motor" droplet is studied in this chapter as a recruiter for other sedentary aqueous droplets to create an asymmetrical network. The polypeptide alamethicin is often used as a voltage-gated channel within DIB networks [18, 19, 40, 42] and is also studied in this chapter. Alamethicin is incorporated in the non-ferrous aqueous phase within an asymmetrical network with an applied sinusoidal voltage. The output current is measured to characterize channel activation.

6.2 Hierarchical Network Manipulation

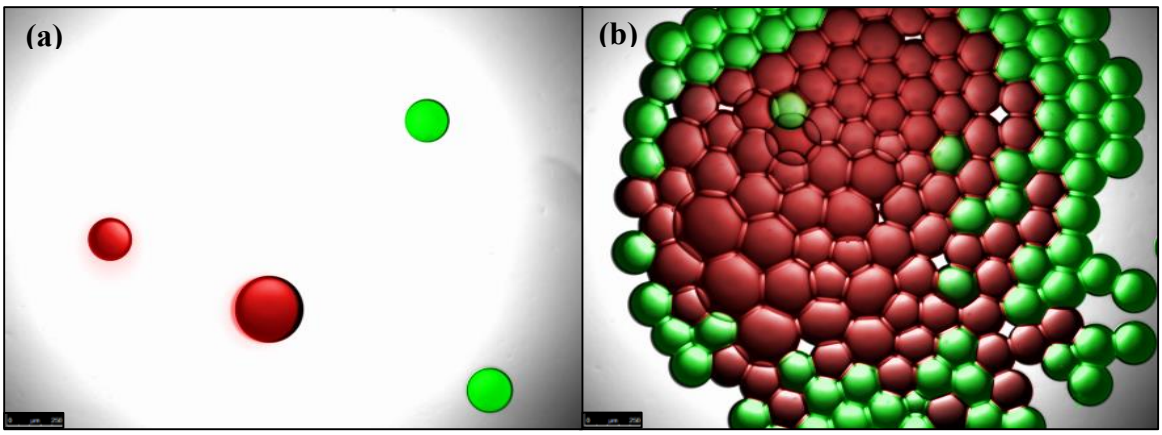

Figure 12: Both droplet varieties were randomly dispersed within an oil reservoir (a). 1.5% (red) droplets were pulled to the center of the cluster, expelling the 0.5% (green) droplets to the exterior. These colored images were created through overlays of fluorescence and DIC images.

Now that it's been proven that ferrous droplets are capable of producing stable membranes while being stretched and reassembled, remote manipulation characteristics are studied. The tip of a pulled pipette (World Precision Instruments, P-1000, Sutter) is filled with ~0.5% volume fraction ferrofluid and another pulled pipette is filled with ~1.5% volume fraction ferrofluid. The two different concentrations of PEG coated ferrofluid droplets were placed in a petri dish (Ibidi) with a 50:50 mixture of hexadecane and silicone oil AR20 (Sigma Aldrich) with dissolved DPhPC phospholipids (Avanti). Fluorescein (Sigma) was added to the 0.5% PEG coated ferrofluid and rhodamine was added to the1.5% PEG-PMMA coated ferrofluid. Both droplet varieties were randomly dispersed within an oil reservoir (Figure 12a). When the magnet was introduced, the 1.5% (red) droplets were pulled to the center of the cluster, expelling the 0.5% (green) droplets to the exterior with the exception of some green droplet that were trapped during the assembly (Figure 12b).This result suggests that the network properties may be tuned through variable ferrofluid composition remotely and even before network assembly.

Once the large network was formed, a magnet was manually moved around the petri dish, and the entire network as able to move freely without any difficulties or membrane failure. This study shows that by tailoring the volume fraction of the ferrofluid, a network can be manipulated even before assembly.

6.3 Motor Droplet

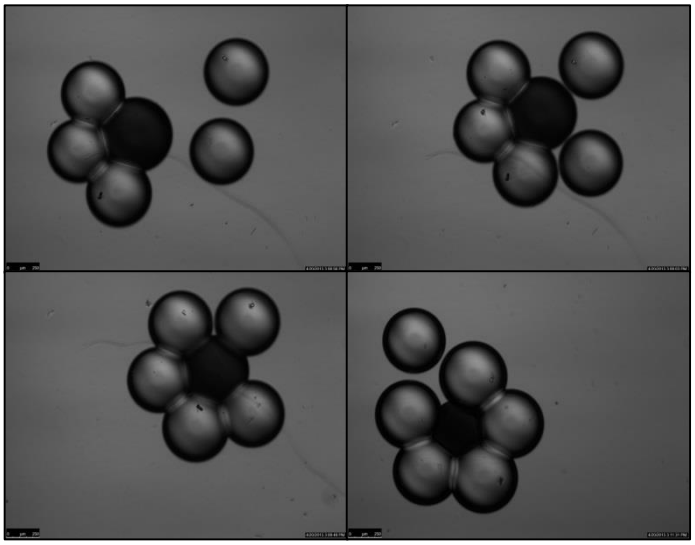

Figure 13: gradual recruitment of an outer ring of non-ferrous droplets through a single motor droplet guided by a magnet.

The ferrofluid droplets require the use of lipids-in-oil for successful DIB formation. This nullifies the use of using DIBs to test membrane proteins or continuing further testing on ion channels. By using a single ferrous droplet as a "motor" droplet to collect various aqueous droplets would still allow for a lipid-in-water approach to continue studies on membrane proteins and ionic channels. The tip of a pulled pipette (World Precision Instruments, P-1000, Sutter) is filled with ~0.5% volume fraction PEG coated ferrofluid. A single ferrous droplet is deposited injected (Femtojet 4i, Eppendorf) into the 50:50 mixture of hexadecane and silicone oil AR20 (Sigma Aldrich) with

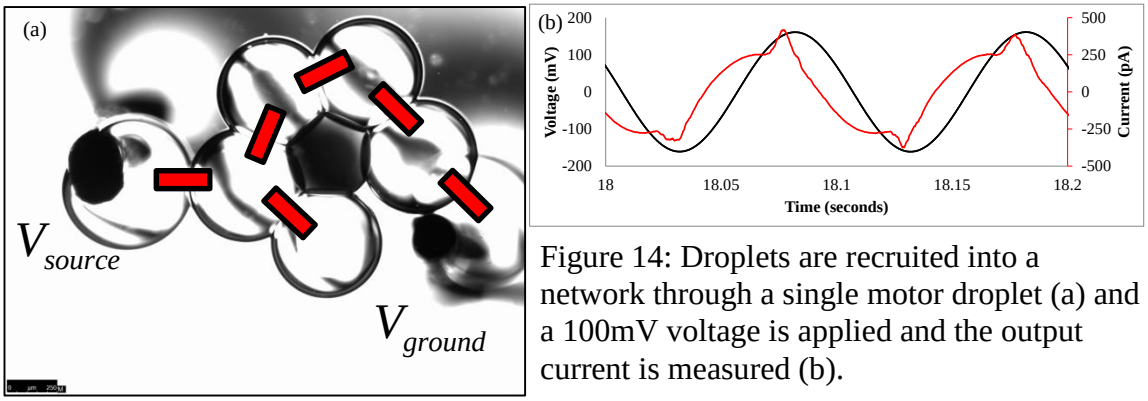

Figure 14: Droplets are recruited into a network through a single motor droplet (a) and a 100mV voltage is applied and the output current is measured (b).

dissolved DPhPC phospholipids (Avanti). Another pulled pipette (World Precision Instruments, P-1000, Sutter) is filled with a DI water buffer solution of 100mM NaCl and 10mM MOPS (Sigma Aldrich) and using the micro injector, various droplets of the same size were arbitrarily deposited in the oil bath. A hand held magnet is used to guide the single ferrous droplet, referred to as a motor droplet, to recruit the other variously placed aqueous droplets in the petri dish. Once a bilayer is formed the ferrous droplet carries both droplets to another aqueous droplet. This sequence continued until a flower or honeycomb shape is formed with six of the aqueous droplets and the ferrous droplet at the center (Figure 13). This process was done first with only lipid-in-oil to confirm that asymmetrical membrane formation was possible. Membrane formation occurred within seconds between ferrous and aqueous droplets. This same process was repeated, this time with the lipids being dissolved in the aqueous phase along with alamethicin. These droplets are recruited into a network through a single motor droplet. The network was then punctured with Ag/AgCl electrodes attached to micromanipulators (Siskiyou) (Figure 14a). The electrodes are connected to a patch-clamp system (Multiclamp 700B, Digidata 1550, and Molecular Devices) and signal generator (Hewlett Packard 33120A). All measurements were taken inside of a Faraday cage to reduce noise. A sinusoidal

voltage is applied and gradually increased. This applied voltage is evenly distributed across the interior membranes of the asymmetrical network. Once the gating threshold is crossed (roughly 40 mV), temporary increases in the conductivity of the membranes are observed (Figure 14b), corresponding to channel activation. This result shows that regular DIB network activity is not hampered by the inclusion of ferrous droplets when they are used for network assembly through asymmetric DIBs. The ability to form asymmetrical membranes will help to enhance the efficiency of creating large networks but still allow for the lipid-in technique to be utilized to continue research on membrane pores and channels.

6.4 Conclusions and Discussion

Remote manipulation is shown to be possible by tailoring the volume fraction of the ferrofluid. Network manipulation is possible pre and post assembly by simply using different volume fraction ferrofluids. In order to advance research on DIBs and propel research onwards to DIBs as an adaptive biologically inspired material, certain fundamental properties must be preserved. One of the primary uses for DIBs as a successful membrane model is the ease at which membrane proteins and channels self-insert in the lipid-in-water technique. As mentioned in Chapter 3, the lipid-in technique posed an issue in membrane formation with would prevent the process of self-insertion. With the success presented in this chapter, asymmetrical networks provide a way to preserve the usefulness of the lipid-in technique and also allow for the utilization of the magnetic responsive property of ferrofluid for rapid network formation and mobility of

the network. A single ferrous droplet has the ability to form asymmetrical networks by recruiting other non-ferrous droplets.

CHAPTER 7

INTERFACIAL TENSION

7.1 Overview

Interfacial tension (IFT) is of upmost importance when characterizing solutions in colloid science. IFT measurements can assess the formation, shape and stability of liquid drops [43, 44]. Interfacial tension is similar to surface tension in that cohesive forces are also involved. However the main forces involved in interfacial tension are adhesive forces (tension) between the liquid phase of one substance and either a solid, liquid or gas phase of another substance. The interaction occurs at the surfaces of the substances involved, that is at their interfaces. By using an open sourced Python code, Open Drop [45], the pendant drop technique will be used to test the IFT of 0.5 % PMMA coated ferrofluid in lipid oil (50:50 mixture of hexadecane and silicone oil AR20 with dissolved DphPC lipids). Measurements for water in lipid oil, ferrofluid in lipid oil, ferrofluid in oil without lipids, and water in oil without lipids are all measured and compared.

7.2 Materials and Methods

The lab engineered a custom set up to take pictures of the drop to measure the IFT. Micromanipulators (Siskiyou) are fastened on to the breadboard of a vibration isolation table (Thorlabs). From the micromanipulator, the injector end of a microinjector is clamped in a vertical position. The microinjector has a capillary tube that the various droplets will be suspended from. A very small portion of the glass is shaded in with a

black marker so the Open Drop software will recognize the boundaries of the capillary tube. Prior to this method of shading in the capillary tube, the software was having some difficulty recognizing the boundary of the capillary tube since the inner portion of the tube is if clear. Another clamp is positioned horizontally under the capillary tube to hold a vial containing the continuous phase for the droplet to be immersed, which in this study was either lipid oil or just the 50:50 mixture of hexadecane and silicon oil AR20 (Sigma Aldrich) with no lipids. A camera (Motic) is horizontally mounted to capture a video or still frames of the drop over time. For a visual representation of the setup, please refer to Appendix A1. The vibration isolation table was leveled prior to the experiments and the custom set up was calibrated by measuring the IFT of deionized (DI) water and air. The calibrated value measured was 68.06 mN/m, which is near previously reported values of water-air surface tension measurements by Vargaftik el al [46]. While the room temperature was 24 Celsius, the light source heated up the water significantly while waiting for the droplet to reach equilibrium, which would explain why the measured value is lower than 71.99 mN/m reported by Vargaftik et al. Once the system is calibrated, a capillary tube is filled with the desired liquid for the drop (either ferrofluid or DI water) and then the tube is inserted at the end of the microinjector. The injector is clamped back into a vertical position and micromanipulators are used to manually submerge the tip of the capillary tube in a plastic vial containing the continuous phase (either lipid oil or oil with no lipids). Then a dial on the micro injector is turned to inflate the drop which will remain undisturbed to reach equilibrium. Each drop is left in the continuous phase for five minutes before video acquisition. Then a video of the drop is taken for one minute the video obtained is then loaded in a Matlab code (Appendix B1)

that will extract still images from the video. The images are then processed in the Open Drop software to calculate the final IFT for each frame. The main principal regrading methods used in this test was the pendant drop technique of measuring IFT and using Open Drop to quantify the results. Both are outlined in further detail in the following section.

7.2.1 Pendant Drop Technique

Pendant drop tensiometry offers a simple solution to determining interfacial tension. Many different techniques have been studied to measure IFT which can be viewed in more detail in a paper by Drelich et al [47]. The pendant drop tensiometry was shown to be the simplest in terms of instrumentation, using just a blunt needle (capillary tube), syringe, light, diffuser for the light source, and a camera to capture the images. The technique involves the acquisition of a silhouette of a fluid droplet and iterative fitting of the Young–Laplace equation that balances gravitational deformation of the drop with the restorative interfacial tension. There are some factors that do pose a problem to the ease of using the pendant drop tensiometry, primarily the balance between interfacial tension and gravitational forces and drop volume. As part of the custom setup to measure IFT, the lab utilizes the open source software Open Drop. Open Drop is a Python code that was programmed to take those issues into account [45]. A pendant drop at equilibrium

$$\mathbf{1 + 1}\boldsymbol{R}\mathbf{2)}=\Delta P\equiv\Delta P0-\Delta\rho gz \qquad (\mathbf{3})$$

which relates the Laplace pressure across an interface and takes into account the curvature of the interface.

$$\gamma \left(\frac{\mathbf{1}}{\boldsymbol{R_1}} + \frac{\mathbf{1}}{\boldsymbol{R_2}}\right) = \Delta P \equiv \Delta P0 - \Delta \rho g z \qquad (3)$$

ΔP is the Laplace pressure across the interface and R_1 and R_2 are the principle radii of the curve, ρ is the density and g is the gravitational acceleration. The Open Drop software can be broken down into two main parts. First the drop profile is extracted from an image, and second, the Young–Laplace equation is iteratively solved to find the physical parameters that most precisely describe the extracted drop profile using optimization techniques. To determine the drop profile, standard edge detection with the Canny edge detector is used [48] because of its robust nature over a range of contrast conditions. Once the droplet profile has been defined, the drop profile is fitted to the extracted experimental data by minimizing the sum of squared residuals and a solution to the Young-Laplace equation is generated. Then for each point the arc-length that minimizes the Euclidean distance is calculated and a Jacobian entry is calculated for each entry point and parameter.

$$\boldsymbol{J_T J} + \boldsymbol{\lambda diag(J_T J))\delta} = \boldsymbol{J_T e} \qquad (4)$$

Then Equation 4 is solved for $\boldsymbol{\delta}$, where $\boldsymbol{e}$ is the vector of residuals and $\boldsymbol{J}$ is the Jacobian matrix. The parameter is updated and then the process is repeated until convergence is reached.

7.3 Results and Conclusions

Three trials were run for each case presented in Table **1** and the measurements of each trial were averaged to obtain the values reported and the standard deviation was also calculated. From the results we see that by including lipids as a surfactant, it greatly reduces the IFT of both DI water and ferrofluid. As mentioned before the lipid-in technique posed some issues in membrane formation. In order to look a little closer in

what may be causing this issue, the IFT of both lipid-in DI water and lipid-in ferrofluid were taken. The average IFT of ferrofluid in oil without lipids was 8.176 mN/m and the lipid-in ferrofluid the IFT was measured to be 9.836 mN/m which is actually about a

	Droplet Profile	Interfacial Tension (mN/m)	Standard Deviation (mN/m)
DI Water in Lipid Oil		1.722	0.096
Ferrofluid in Lipid Oil		2.061	.0132
DI Water in Oil		10.99	0.793
Ferrofluid in Oil		8.176	0.154
Lipid-In DI Water in Oil		1.427	0.125
Lipid-in Ferrofluid in Oil		9.836	0.451

Table 1: Three trials were run for each case and the average of the trials is reported along with the standard deviation and an image of the droplet profile that was used to calculate the IFT.

20% increase in IFT which goes against fundamental properties of lipids as a surfactant. This gives a little bit of insight as to why the lipid-in technique does not work for ferrofluid; perhaps the lipids are self-asserting onto the nanoparticles in the ferrofluid

instead of forming a monolayer on the interface of the drop and continuous phase. More research should be done on the PMMA coating of the ferrofluid to fully understand how and where the lipids are inserting. However, for the ferrofluid in lipid oil measurement a 75% decrease in IFT was observed from the IFT of ferrofluid in oil without lipids which is what is expected. From these results we can see that the lipid-in oil technique is not interfering with monolayer formation and the expected decrease in IFT is observed throughout trials. Dynamic measurements of IFT were taken as well as the equilibrium IFT for ferrofluid in lipid oil. The dynamic IFT can show the rate of lipid insertion on a drop. For the lipid-in oil technique, the rate of insertion was faster than the lab had anticipated. Once the drop was inflated, the insertion happens almost instantly which made it difficult to capture the initial decay of the IFT. The pendant drop technique may not be the most ideal method to capture the dynamic IFT mainly due to the fact that the time step is less than one second for this situation, but by using the MATLab code to convert a video into still frames, dynamic IFT can be measured (Figure 15).

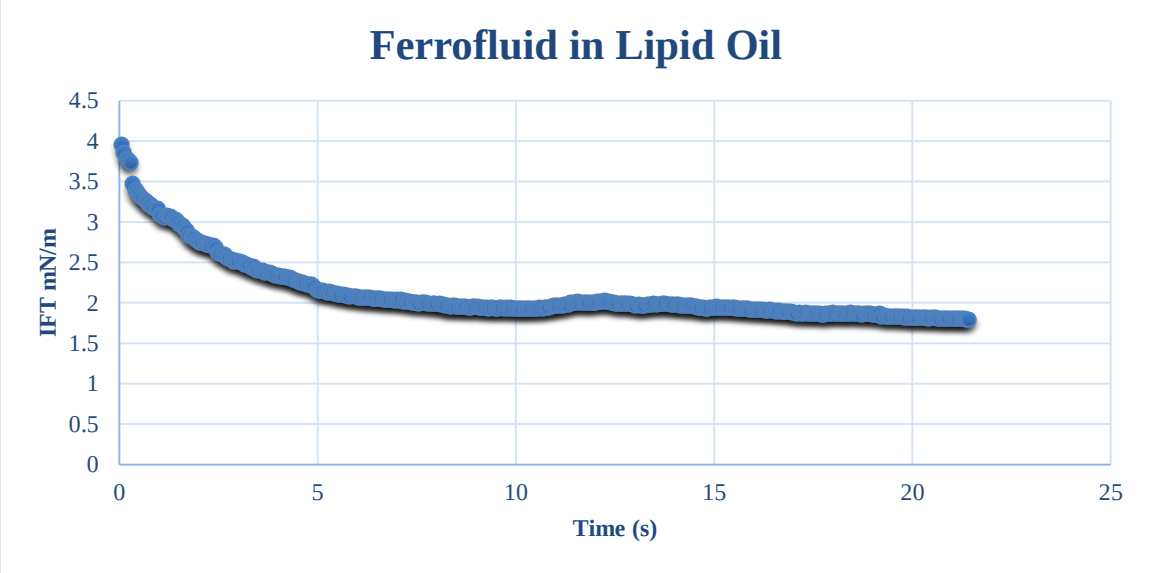

Figure 15: Graph of the dynamic IFT of ferrofluid in lipid oil.

CHAPTER 8

CONCLUSION AND DISCUSSION

8.1 Closing Discussion

The DIB technique has revolutionized the field for studying artificial membranes. It provides a simple and elegant solution for creating a stable lipid bilayer. The ability to create interconnected membranes makes it an attractive model to advance research on ion channels, membrane proteins, and studying cardiac tissue, and even 3D printing organs. However the process of creating an extensive network of such caliber requires the need for a more streamlined approach. Currently the methods used and extracting real biological membranes are tedious and time consuming. The work looked to solve this limitation by incorporating ferrofluid in the aqueous phase of membrane creation. By utilizing the magnetic properties of ferrofluid, large DIB networks can be created by the use of a magnet. First the ferrofluid in question, needs to be biocompatible. By using a biocompatible ferrofluid, the option to use a DIB *in vivo* is still an option. Polyethylene glycol (PEG) and polymethyl methacrylate (PMMA) are biocompatible coatings that coated the nanoparticles in the ferrofluid used in the experiments. In order fully develop a protocol for ferrous network creation, further research needs to be done to certify that the properties of a stable, healthy bilayer were not hindered by the inclusion of ferrofluid in the aqueous phase. When trying the lipid-in technique where lipids were dissolved in the ferrofluid, it was quickly realized that membrane formation was not occurring properly.

This scenario was further researched by measuring the interfacial tension of a lipid-in ferrofluid drop. A lipid surfactant will decrease the overall tension of the drop when properly coasted. The opposite was observed for a lipid-in ferrofluid drop. This could perhaps be due to the lipids self-asserting on the magnetic particles in the ferrofluid, rather than forming a monolayer at the ferrofluid-oil interface. However, when the lipids were dissolved in the continuous oil phase, the membrane formation happened remarkably fast. Once it was visually assessed that membrane formation occurred, the membrane was then characterized. First a test to ensure that the membranes formed were not leaky fluorescein dye was added to half of the droplets and a network was formed. Then a fluorescent image was taken to check for any leakage of dye and no leakage was detected between the membranes in the network. To characterize the ferrous membranes further, specific capacitance measurements were taken and compared to previously reported values of aqueous membranes. It was found that the ferrous DIB was $0.82 \pm 0.078 \mu F/cm^2$ and $0.77 \pm 0.078\ \mu F/cm^2$ for the aqueous droplets. These values are in close agreement with previously reported values of $0.65 \pm 0.2 \mu F/cm^2$ and $0.64 \pm 0.003 \mu F/cm^2$ for a DIB formed using hexadecane. Since our measurements were taken in a 50:50 mixture of hexadecane and silicone oil, the values were expected to be slightly higher. Ferrous DIBs showed to exhibit similar specific capacitance measurements to that of aqueous membranes with the values of both being within the standard deviation of each other. After characterizing a single DIB, networks were then examined. A very similar capacitance test was performed on a large ferrous network. The network was stretched and manipulated while electrical measurements were taken. The ferrous network showed incredible flexibility in reconfiguring when manually manipulated. Remote manipulation

was also tested both pre and post assembly. For pre assembly manipulation, two different ferrofluids with different volume fraction were deposited in a petri and when a handheld magnet was placed in under the petri dish, the network assembled with the higher volume fraction ferrofluid in the center with the lower volume fraction on the outside. This tailoring of volume fraction could allow for pre assembly manipulation of a network. Remote manipulation was also shown to be possible by moving the network with a handheld magnet, and by the use of manual micromanipulators.

DIBs have become the go to membrane model to study membrane proteins, ionic channels, and other membrane phenomena. The inclusion of ferrofluid in the aqueous phase which requires a lipid-out technique, whereas in order for a membrane protein or channel to self-insert into a membrane, the lipids must be dissolved in the aqueous phase. In order to still have the benefits of ferrofluid and the ability to study membrane proteins and channels, asymmetrical membranes were studied. A single ferrous droplet was deposited in a petri dish and used a “motor” droplet to recruit other non-ferrous droplets throughout the petri dish. Membranes were formed and were easily maneuvered throughout the petri dish. Alamethicin was then incorporated in an asymmetrical network to assess the electrical characteristics of having asymmetrical bilayers. It was shown that the alamethicin channel was not hindered, the membrane showed temporary increases in conductivity, corresponding to channel activation. Lastly interfacial tension measurements were taken for both ferrous and aqueous drops and compared. The lipid in oil trials for both drops showed the expected decrease in IFT that has been previous reported when compared to the IFT of the drop in oil sans lipids. From the research in the work, it is clear that ferrofluid has little interference with membrane formation to create

networks and asymmetrical networks. By incorporating ferrofluid into the aqueous phase, not only is network assembly made simpler, but remote manipulation is also made possible. Creating a more rapid solution to creating complex DIB networks could open the door for applying this technique to study transmembrane proteins, creating a biologically adaptive material, and perhaps advancing towards the tissue scale in the future.

REFERENCES

1. Freeman, E., et al., *The mechanoelectrical response of droplet interface bilayer membranes.* Soft matter, 2016. **12**(12): p. 3021-3031.
2. Edidin, M., *Lipids on the frontier: a century of cell-membrane bilayers.* Nature Reviews Molecular Cell Biology, 2003. **4**(5): p. 414-418.
3. Ottova, A. and H. Tien, *The Lipid Bilayer Principle: A Historic Perspective and Some Highlights.* Advances in Planar Lipid Bilayers and Liposomes, 2005. **1**: p. 1-76.
4. Lewis, B.A. and D.M. Engelman, *Lipid bilayer thickness varies linearly with acyl chain length in fluid phosphatidylcholine vesicles.* Journal of molecular biology, 1983. **166**(2): p. 211-217.
5. Benz, R. and K. Janko, *Voltage-induced capacitance relaxation of lipid bilayer membranes Effects of membrane composition.* Biochimica et Biophysica Acta (BBA)-Biomembranes, 1976. **455**(3): p. 721-738.
6. Raguse, B., et al., *Tethered lipid bilayer membranes: formation and ionic reservoir characterization.* Langmuir, 1998. **14**(3): p. 648-659.
7. Schoch, P., D.F. Sargent, and R. Schwyzer, *Capacitance and conductance as tools for the measurement of asymmetric surface potentials and energy barriers of lipid bilayer membranes.* The Journal of membrane biology, 1979. **46**(1): p. 71-89.

8. Taylor, G.J., et al., *Direct in situ measurement of specific capacitance, monolayer tension, and bilayer tension in a droplet interface bilayer.* Soft matter, 2015. **11**(38): p. 7592-7605.

9. Needham, D. and R.S. Nunn, *Elastic deformation and failure of lipid bilayer membranes containing cholesterol.* Biophysical journal, 1990. **58**(4): p. 997.

10. Mruetusatorn, P., et al., *Dynamic morphologies of microscale droplet interface bilayers.* Soft matter, 2014. **10**(15): p. 2530-2538.

11. Mueller, P., et al., *Methods for the formation of single bimolecular lipid membranes in aqueous solution.* The Journal of Physical Chemistry, 1963. **67**(2): p. 534-535.

12. Mueller, P., et al., *Reconstitution of cell membrane structure in vitro and its transformation into an excitable system.* Nature, 1962. **194**: p. 979-980.

13. Montal, M. and P. Mueller, *Formation of bimolecular membranes from lipid monolayers and a study of their electrical properties.* Proceedings of the National Academy of Sciences, 1972. **69**(12): p. 3561-3566.

14. Holden, M.A., D. Needham, and H. Bayley, *Functional bionetworks from nanoliter water droplets.* Journal of the American Chemical Society, 2007. **129**(27): p. 8650-8655.

15. Hwang, W.L., et al., *Electrical behavior of droplet interface bilayer networks: experimental analysis and modeling.* Journal of the American Chemical Society, 2007. **129**(38): p. 11854-11864.

16. Funakoshi, K., H. Suzuki, and S. Takeuchi, *Lipid bilayer formation by contacting monolayers in a microfluidic device for membrane protein analysis.* Analytical chemistry, 2006. **78**(24): p. 8169-8174.

17. Hwang, W.L., et al., *Asymmetric droplet interface bilayers.* Journal of the American Chemical Society, 2008. **130**(18): p. 5878-5879.

18. Bayley, H., et al., *Droplet interface bilayers.* Molecular BioSystems, 2008. **4**(12): p. 1191-1208.

19. Sarles, S.A. and D.J. Leo, *Tailored current-voltage relationships of droplet-interface bilayers using biomolecules and external feedback control.* Journal of intelligent material systems and structures, 2009.

20. Xu, J., F.J. Sigworth, and D.A. LaVan, *Synthetic protocells to mimic and test cell function.* Advanced Materials, 2010. **22**(1): p. 120-127.

21. Creasy, M. and D. Leo, *Non-invasive measurement techniques for measuring properties of droplet interface bilayers.* Smart materials and structures, 2010. **19**(9): p. 094016.

22. Sarles, S.A. and D.J. Leo, *Regulated attachment method for reconstituting lipid bilayers of prescribed size within flexible substrates.* Analytical chemistry, 2010. **82**(3): p. 959-966.

23. Sarles, S.A. and D.J. Leo, *Physical encapsulation of droplet interface bilayers for durable, portable biomolecular networks.* Lab on a Chip, 2010. **10**(6): p. 710-717.

24. Shearman, G.C., et al., *A 3-D hexagonal inverse micellar lyotropic phase.* Journal of the American Chemical Society, 2009. **131**(5): p. 1678-1679.

25. Tsofina, L., E. Liberman, and A. Babakov, *Production of bimolecular protein-lipid membranes in aqueous solution.* 1966.

26. Syeda, R., et al., *Screening blockers against a potassium channel with a droplet interface bilayer array.* Journal of the American Chemical Society, 2008. **130**(46): p. 15543-15548.

27. Wauer, T., et al., *Construction and Manipulation of Functional Three-Dimensional Droplet Networks.* ACS nano, 2014. **8**(1): p. 771-779.

28. Villar, G., A.D. Graham, and H. Bayley, *A tissue-like printed material.* Science, 2013. **340**(6128): p. 48-52.

29. Stanley, C., et al., *A microfluidic approach for high-throughput droplet interface bilayer (DIB) formation.* Chemical communications, 2010. **46**(10): p. 1620-1622.

30. Kose, A.R., et al., *Label-free cellular manipulation and sorting via biocompatible ferrofluids.* Proceedings of the National Academy of Sciences, 2009. **106**(51): p. 21478-21483.

31. Zhu, T., F. Marrero, and L. Mao, *Continuous separation of non-magnetic particles inside ferrofluids.* Microfluidics and nanofluidics, 2010. **9**(4-5): p. 1003-1009.

32. Zhu, T., et al., *Continuous-flow ferrohydrodynamic sorting of particles and cells in microfluidic devices.* Microfluidics and nanofluidics, 2012. **13**(4): p. 645-654.

33. Hiergeist, R., et al., *Application of magnetite ferrofluids for hyperthermia.* Journal of Magnetism and Magnetic Materials, 1999. **201**(1): p. 420-422.

34. Zhao, Q., et al., *Magnetic nanoparticle-based hyperthermia for head & neck cancer in mouse models.* Theranostics, 2012. **2**(1): p. 113.

35. Gangopadhyay, P., et al., *Novel superparamagnetic core (shell) nanoparticles for magnetic targeted drug delivery and hyperthermia treatment.* Magnetics, IEEE Transactions on, 2005. **41**(10): p. 4194-4196.

36. Liu, T.-Y., et al., *Preparation and characterization of thermal-sensitive ferrofluids for drug delivery application.* Journal of Magnetism and Magnetic Materials, 2007. **310**(2): p. 2850-2852.

37. Mahmoudi, M., et al., *Superparamagnetic iron oxide nanoparticles (SPIONs): Development, surface modification and applications in chemotherapy.* Advanced Drug Delivery Reviews, 2011. **63**(1–2): p. 24-46.

38. Scherer, C. and A.M. Figueiredo Neto, *Ferrofluids: properties and applications.* Brazilian Journal of Physics, 2005. **35**(3A): p. 718-727.

39. Rosensweig, R.E., *Ferrohydrodynamics*. 2013: Courier Corporation.

40. Nguyen, M.-A. and S.A. Sarles. *Micro-Encapsulation and Tuning of Biomolecular Unit Cell Networks*. in *ASME 2014 Conference on Smart Materials, Adaptive Structures and Intelligent Systems*. 2014. American Society of Mechanical Engineers.

41. Creasy, M.A., et al., *Deterministic model of biomolecular networks with stimuli-responsive properties.* Journal of Intelligent Material Systems and Structures, 2014: p. 1045389X14536004.

42. Bruner, L. and J. Hall, *Pressure effects on alamethicin conductance in bilayer membranes.* Biophysical journal, 1983. **44**(1): p. 39.

43. Eggers, J., *Nonlinear dynamics and breakup of free-surface flows.* Reviews of Modern Physics, 1997. **69**(3): p. 865-930.

44. Eggers, J. and E. Villermaux, *Physics of liquid jets.* Reports on progress in physics, 2008. **71**(3): p. 036601.

45. Berry, J.D., et al., *Measurement of surface and interfacial tension using pendant drop tensiometry.* Journal of Colloid and Interface Science, 2015.

46. Vargaftik, N., *International Tables of the Surface Tension of Water*. 1983.

47. Drelich, J., C. Fang, and C. White, *Measurement of interfacial tension in fluid-fluid systems.* Encyclopedia of surface and colloid science, 2002. **3**: p. 3158-3163.

48. Canny, J., *A Computational Approach to Edge Detection.* IEEE Transactions on Pattern Analysis and Machine Intelligence, 1986. **PAMI-8**(6): p. 679-698.

APPENDIX

APPENDIX A: EXPERIMENTAL SET UP

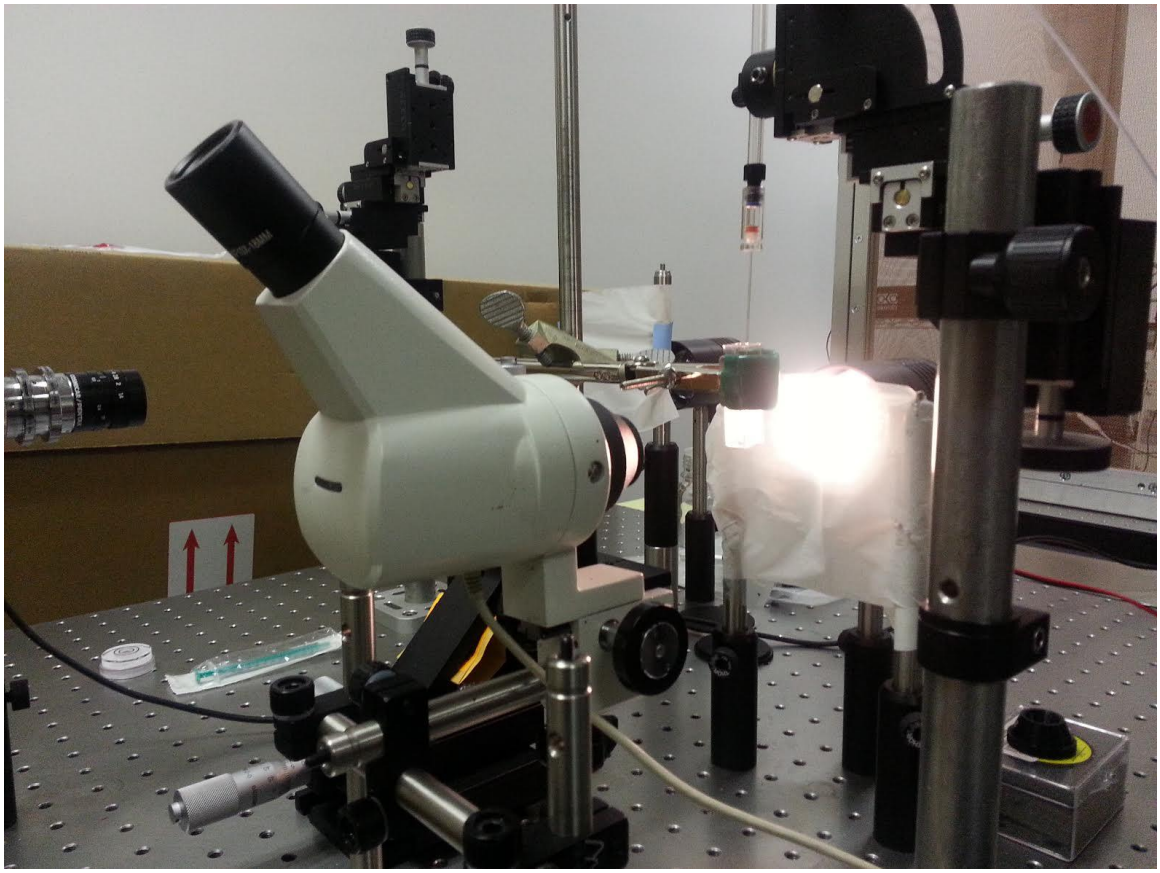

Appendix A1: Custom set up for IFT measurements using pendant drop tensiometry

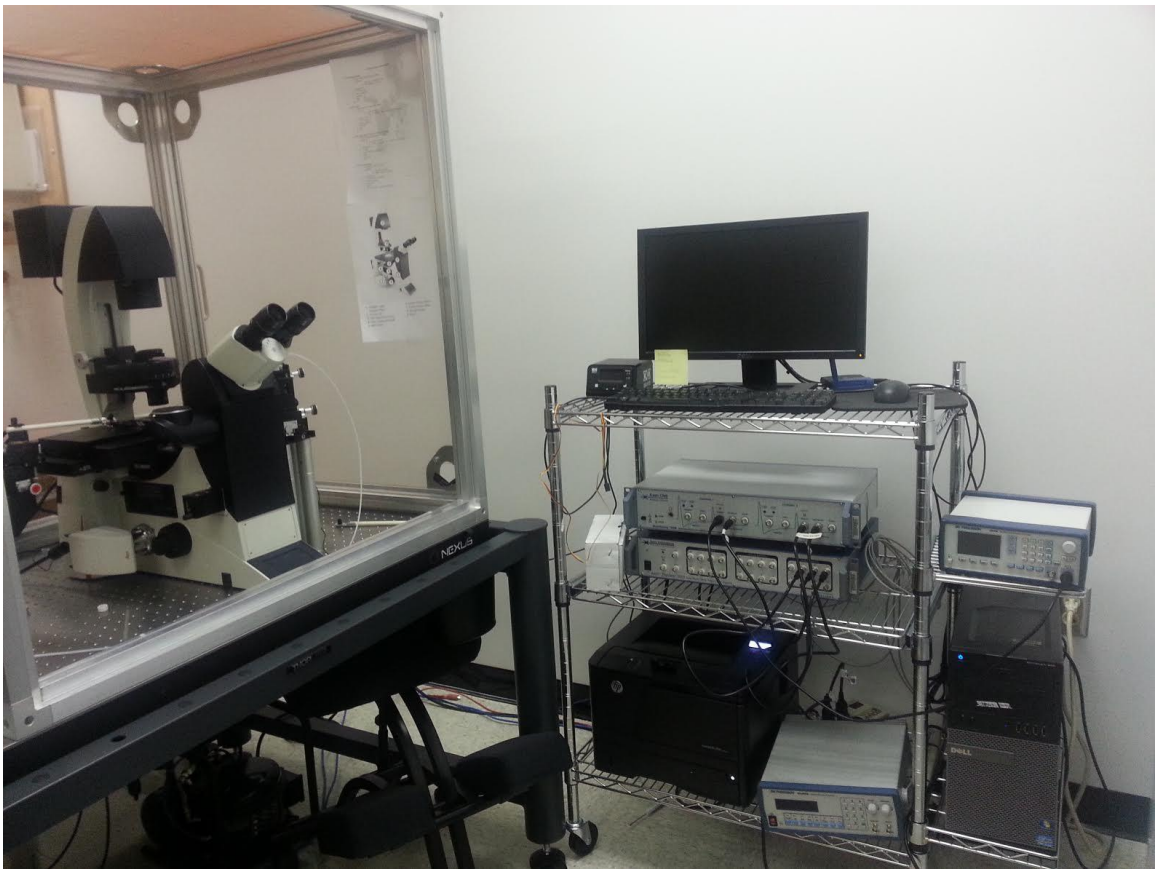

Appendix A2: Lab set up to take capacitance measurements

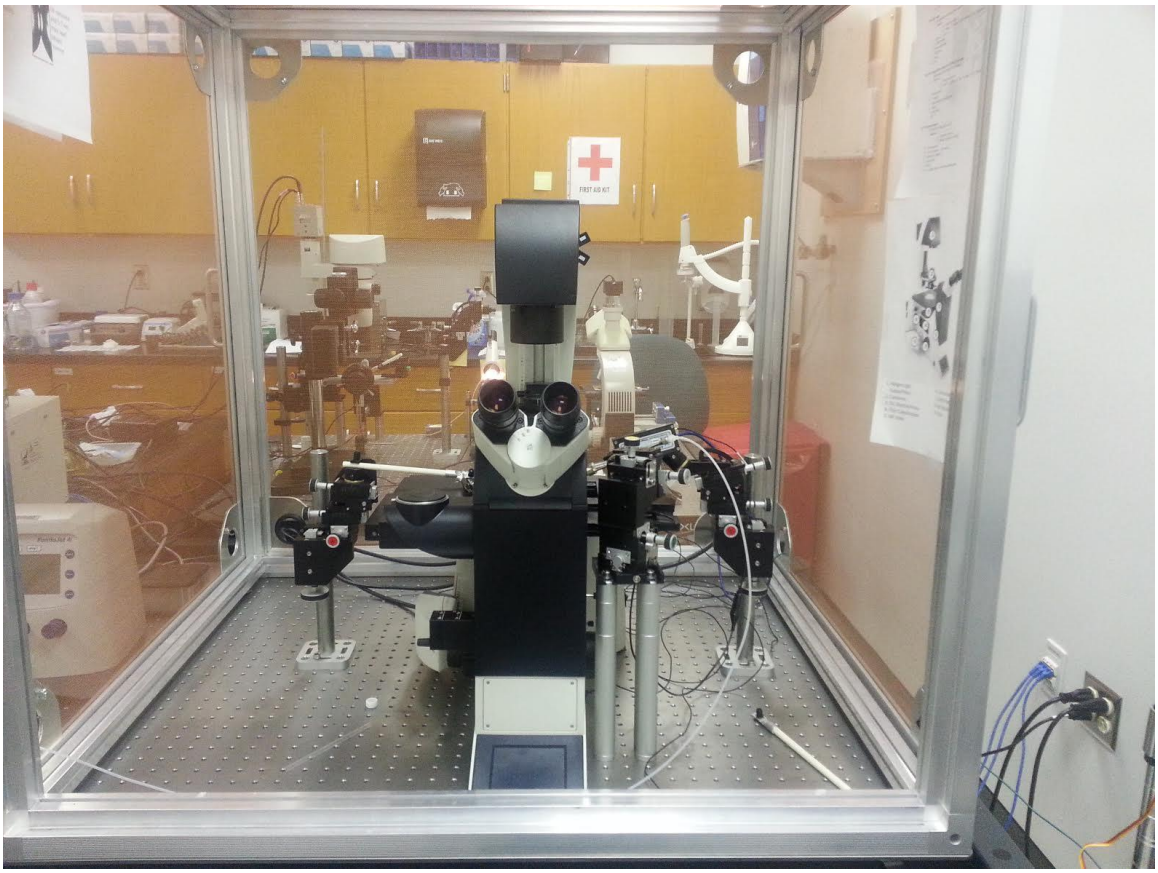

Appendix A3: Lab set up to take capacitance measurements. Close up of microscope used.

APPENDIX B: MATLAB CODE

```
%This script will export your Thorcam .avi files to multiple still
images
%(one image for each frame).  Be sure to track your set fps in thorcam
so
%you know the time lapse between each - currently I have set it to 10,
but
%I'm certain you can improve it.

workingDir = 'C:\Users\khushb89\Desktop\ThorCam';
%mkdir(workingDir)
%mkdir(workingDir,'images');

dropVideo=VideoReader('water.avi');

ii = 1;

while hasFrame(dropVideo)
   img = readFrame(dropVideo);
   filename = [sprintf('%03d',ii) '.jpg'];
   fullname = fullfile(workingDir,'images',filename);
   imwrite(img,fullname)    % Write out to a JPEG file (img1.jpg,
img2.jpg, etc.)
   ii = ii+1;
end
```

Appendix B1: Matlab code to extract still images from an avi file.